

Regulation of Varicella-Zoster Virus-Induced Cell-to-Cell Fusion by the Endocytosis-Competent Glycoproteins gH and gE

Tracy Jo Pasieka,¹ Lucie Maresova,¹ Kimiyasu Shiraki,² and Charles Grose^{1*}

Department of Pediatrics, University of Iowa College of Medicine, Iowa City, Iowa,¹ and Department of Virology, Toyama Medical and Pharmaceutical University, Toyama, Japan²

Received 25 August 2003/Accepted 20 November 2003

The gH glycoprotein of varicella-zoster virus (VZV) is a major fusogen. The realigned short cytoplasmic tail of gH (18 amino acids) harbors a functional endocytosis motif (YNKI) that mediates internalization in both VZV-infected and transfected cells (T. J. Pasieka, L. Maresova, and C. Grose, *J. Virol.* 77: 4194-4202, 2003). During subsequent confocal microscopy studies of endocytosis-deficient gH mutants, we observed that cells transfected with the gH tail mutants exhibited marked fusion. Therefore, we postulated that VZV gH endocytosis served to regulate cell-to-cell fusion. Subsequent analyses of gH+gL transfection fusion assays by the Kolmogorov-Smirnov statistical test demonstrated that expression of the endocytosis-deficient gH mutants resulted in a statistically significant enhancement of cell-to-cell fusion ($P < 0.0001$) compared to wild-type gH. On the other hand, coexpression of VZV gE, another endocytosis-competent VZV glycoprotein, was able to temper the fusogenicity of the gH endocytosis mutants by facilitating internalization of the mutant gH protein from the cell surface. When the latter results were similarly analyzed, there was no longer any enhanced fusion by the endocytosis-deficient gH mutant protein. In summary, these studies support a role for gH endocytosis in regulating the cell surface expression of gH and thereby regulating gH-mediated fusion. The data also confirm and extend prior observations of a gE-gH interaction during viral glycoprotein trafficking in a VZV transfection system.

Varicella-zoster virus (VZV) is an extremely cell-associated alphaherpesvirus. Unlike many herpesviruses, VZV is not released into the medium overlying cultured cells (15, 50). Instead, the virus spreads through fusion of one infected cell plasma membrane to that of an adjacent cell. Syncytium formation is induced by the expression of fusogenic viral glycoproteins and results in the formation of large polykaryons that can include hundreds of nuclei (19). We have previously documented cell-to-cell fusion in transfected HeLa cells coexpressing gH and gL (11, 30). For the related herpes simplex virus type 1 (HSV-1) and HSV-2, syncytium formation requires expression of the quartet gH, gL, gD, and gB (48). Pseudorabies virus and human herpesvirus type 8 fusion require the coexpression of gH, gL, and gB, but not gD (26, 43). Of further interest, other glycoproteins may further modulate virus induced fusion activity (1).

All wild-type strains of VZV are highly fusogenic within human skin cells at the base of the typical vesicular lesions of chickenpox, as well as in cultured cells. Studies conducted in this laboratory over several years have demonstrated that the amount of VZV fusion in cell culture is affected by at least three factors: incubation temperature, cell type, and virus strain (8). Fusion was found to be more prominent in epidermal cells and neuroectodermally derived human melanoma cells than in fibroblasts. In addition, when the amount of fusion was compared at 37°C versus 33°C, cells incubated at the lower temperature were markedly more fused. Finally, viruses with mutations in the gE ectodomain have altered spread and fusion properties (16, 45). In order to dissect these fusion

parameters, subsequent studies are being conducted with individual viral glycoproteins under transient-transfection conditions.

The major VZV fusogen gH is a type I glycoprotein originally called gp118 and then called gpIII. VZV gH is transported to and inserted within the plasma membrane, where it presumably would remain throughout the infectious cycle. However, in an unexpected finding, VZV gH was recently demonstrated to undergo endocytosis in both VZV-infected and gH + gL-transfected cells via a tyrosine-based endocytosis signal (42). The YNKI motif had gone unrecognized because of a misalignment in the length of the endodomain. Given the known fusogenic nature of VZV gH, we postulated that the newly discovered endocytic property of gH may play a role in regulating cell surface expression of gH.

We describe here significantly increased levels of cell-to-cell fusion when the gH endocytosis mutants are expressed in a transfection system and compared to the wild-type gH glycoprotein. Further, VZV gE is shown to temper cell-to-cell fusion and cell surface expression of the gH endocytosis mutants through coendocytosis of a gE:gH complex. From these data, we propose that endocytosis of VZV gH regulates the levels of cell-to-cell fusion by controlling the cell surface density of the fusogenic gH protein. Given that syncytium formation is such a prominent feature of *in vivo* infection, endocytosis of VZV gH may be a mechanism by which the virus can modulate this property.

MATERIALS AND METHODS

Cells, plasmids, and viruses. HeLa cells (ATCC CCL-2) were maintained as previously reported (52). For individual or combined glycoprotein expression in HeLa cells, a T7-driven vector pTM1 was utilized. Vaccinia virus expressing the T7 polymerase (VV-T7) was obtained from the Bernard Moss laboratory (36).

* Corresponding author. Mailing address: University of Iowa Hospital/2501 JCP, 200 Hawkins Dr., Iowa City, IA 52242. Phone: (319) 356-2270. Fax: (319) 356-4855. E-mail: charles-grose@uiowa.edu.

Construction of pTM1 vectors has been previously described: pTM1-gE (52), pTM1-gE-tailless (53), pTM1-gB (29), pTM1-gH and pTM1-gL (11, 13), pTM1-gL.13 (45), and pTM1-gH-Y835A and pTM1-gH-S830stop (42).

Antibodies and fluoroprobes. Murine monoclonal antibody (MAb) 258 detects both immature and mature glycosylated VZV gH (10, 11). Murine MAb 206 recognizes only a conformation-dependent epitope on the fully mature form of gH (35). Human MAb V3 (also called Ti-57) is directed against a conformational epitope on mature gH, whereas human MAb V1 recognizes gB (47, 54). Murine MAb 3B3 binds to a well-characterized linear epitope in the ectodomain of gE (17, 20, 45). Murine MAb 158 is directed against gB (34). One additional murine MAb to gH was purchased from Biodesign, Saco, Maine. Fluoroconjugated goat anti-human Alexa 488, goat anti-mouse Texas Red-X, and goat anti-mouse Alexa 488 were the secondary reagents for confocal analysis of VZV glycoproteins (Molecular Probes, Eugene, Oreg.).

Transfection protocols. For transfection with the T7-driven pTM1 vector, HeLa cells were first infected with VV-T7 (36). The cells were subsequently transfected with 3 μ g of each glycoprotein vector with the FuGENE-6 transfection reagent according to the kit protocol (Roche, Indianapolis, Ind.). Monolayers transfected with pTM1 were processed 18 h posttransfection.

Steady-state laser scanning confocal microscopy assay. The subcellular location of glycoproteins was investigated with a steady-state confocal microscopy assay (42). Briefly, transfected cells cultured on glass coverslips were fixed with 2% paraformaldehyde for 60 min. If permeabilization was required, 0.05% Triton X-100 was added during fixation. Samples were incubated with the indicated glycoprotein specific primary antibodies, followed by fluoroconjugated secondary antibodies. Samples were mounted in Mowiol (Calbiochem, San Diego, Calif.) containing 10% 1,4-diazabicyclo(2,2,2)octane on glass slides and viewed with a Zeiss 510 laser scanning confocal microscope (Carl Zeiss, Gottingen, Germany). In the examination of gH cytoplasmic and surface expression, to ensure that each sample received similar transfection and processing treatments, the cells were cultured on 20-by-20-mm glass coverslips. Before fixation, one transfected coverslip was quartered to give both a permeabilized and a nonpermeabilized sample for individual analysis with MAb 258 and MAb 206.

Antibody-mediated inhibition of fusion. HeLa cells were transfected as specified, and then 40 μ l of MAb 206 was added to samples at 4 h posttransfection. As controls, no antibody or 40 μ l of MAb 3B3 was added to similarly transfected cultures. Samples were incubated overnight at 37°C. At 18 h posttransfection, samples were processed for the steady-state endocytosis assay with permeabilization, with MAb 258 and goat anti-mouse Alexa 488 to detect gH+gL-transfected cells.

Assay of glycoprotein endocytosis by laser scanning confocal microscopy. Investigation of glycoprotein endocytosis was carried out as previously described (42). Briefly, primary antibodies were added to cold Hanks balanced salt solution for 1 h at 4°C to label surface glycoproteins. After a washing step, samples were returned to 37°C for the specified amounts of time. After fixation and permeabilization, the appropriate secondary antibodies were applied to fluorolabel the internalized glycoprotein within cytoplasmic vesicles.

Area determination of syncytia by point counting method. Images from transfected HeLa cells labeled with MAb 258 and the Alexa 488 fluoroprobe were collected at low magnification ($\times 20$). Each transfection condition was repeated three times, and 30 random photos were collected from each condition, giving a total of 90 photos. Generally images were collected from a coverslip by first progressing in a left-to-right pattern and then in a right-to-left pattern until 30 images were obtained. The point counting method (28, 38) was used for area determination of each syncytium examined as previously described (41). Briefly, a grid containing systematically positioned lattice points on transparency paper was placed over randomly acquired $\times 20$ micrographs of transfected cells labeled for gH. Points were counted as positive if the profile area fell within the syncytial perimeter defined by fluorolabeled gH. Only syncytia with four or more points were counted. The accuracy of this method in measuring syncytial area was verified by using the software attached to the confocal microscope (Carl Zeiss LSM510, version 3.2). In our study, one point equaled 225 μ m². Median syncytium sizes were calculated with Microsoft Excel.

Kolmogorov-Smirnov statistical analysis of syncytial size. The point counting data were analyzed manually with the Kolmogorov-Smirnov test, as recently described (23, 41). Briefly, the number of syncytia that fell into each user-defined rank size (see Table 1, tally column) and the cumulative number at each rank (cumulative column) were determined. The cumulative proportion (C proportion column) was determined through division of the cumulative number per rank by the total number of syncytia in a sample set. The maximum absolute difference (D) between the cumulative proportions of two samples was determined and used in the calculation of λ with the equation $\lambda = D(mn/m + n)^{1/2}$, where m and n are the two population sizes for the samples being compared. The

TABLE 1. VZV gH cytoplasmic tail sequences

Cytoplasmic tail	Sequence ^a	Reference
gH-wt	WMLCGNSRLREYNKIPLT	11, 13
gH-Y835A	WMLCGNSRLRE <u>AN</u> KIPLT	42
gH-S830stop	WMLCGN	42
gH-bt	WMLCGN <u>KRSR</u> KYKIPLT	10

^a Mutations from wild-type gH are underlined and are based on GenBank sequences no. NC 001348 and AY005331.

cumulative probability (Q) for a given λ was derived from a table provided by Hollander and Wolfe (23). Subtraction of the cumulative probability from 1 gave the two-tailed P value for the two compared samples. P values falling below 0.5 indicated that the data failed the normality test; such values were considered significant. The results are shown for three replicate experiments from each transfection condition. For a visual representation of the results, the numbers were plotted with the point values on the x axis and the cumulative percentages on the y axis.

Biotinylation of cell surface gH. Transfected HeLa monolayers were washed three times with cold 10 mM borate buffer (pH 8.8) containing 0.1 M NaCl. To each 35-mm well, 7.5 μ l of NHS-LC biotin (Pierce, Rockford, Ill.) in 1 ml of borate buffer was added, followed by incubation for 20 min at 4°C. Thereafter, the solution was replaced with an identical fresh solution, and the labeling reaction was continued for 15 min at 4°C. Monolayers were then washed once with cold borate buffer. The biotinylation reaction was stopped by the addition of 10 mM NH₄Cl solution for 20 min at 4°C. The cells were washed four times with 50 mM Tris-HCl (pH 7.2)–0.1 M NaCl. The labeled monolayers were harvested in radioimmunoprecipitation assay buffer with inhibitors, and immunoprecipitation was performed as specified with either 1 μ l of MAb V3 or 4 μ l of MAb 3B3. Samples were subjected to sodium dodecyl sulfate–8% polyacrylamide gel electrophoresis (SDS–8% PAGE) under nonreducing conditions. Immunoprecipitated and biotinylated gH was detected with streptavidin-horseradish peroxidase (HRP) by Western blotting using standard procedures (10, 17). Films with grayscale bands were analyzed with the Kodak Image Analysis Software (Eastman Kodak Company, Rochester, N.Y.).

RESULTS

Imaging of endocytosis and fusion with two gH endocytosis mutants. VZV gH has fusogenic activities that induce cell-to-cell fusion when coexpressed with gL (11, 35, 44). Further, VZV gH undergoes endocytosis in both VZV-infected and gH+gL-transfected cells (42). In our prior study of gH endocytosis, we constructed two gH mutants, gH-Y835A and gH-S830stop, both of which are endocytosis deficient (42). As a control for potential conformational changes due to mutagenesis of the gH cytoplasmic tail, we included a previously constructed gH mutant (gH-basic tail [bt]) (10). The cytoplasmic tail sequences of the four gH proteins are presented in Table 1.

To begin, we compared endocytosis in the four gH constructs coexpressed with VZV gL after a 60-min endocytosis time point (Fig. 1A to D). As previously reported, VZV gH internalized after 60 min at 37°C and accumulated in vesicles in the cytoplasm (Fig. 1A). In contrast, the gH endocytosis mutants gH-Y835A and gH-S830stop coexpressed with gL did not internalize; thus, they retained a halo pattern of staining (Fig. 1C and D, respectively). The gH-bt+gL construct underwent endocytosis from the plasma membrane (Fig. 1B) in a characteristic vesicular pattern resembling the results with gH-wild type (wt)+gL.

We observed increased levels of cell-to-cell fusion in our analyses of the gH endocytosis mutants. To examine this phenomenon in greater detail, HeLa cells were cotransfected as described above, processed for the steady-state confocal assay, and examined at low magnification to generate landscape im-

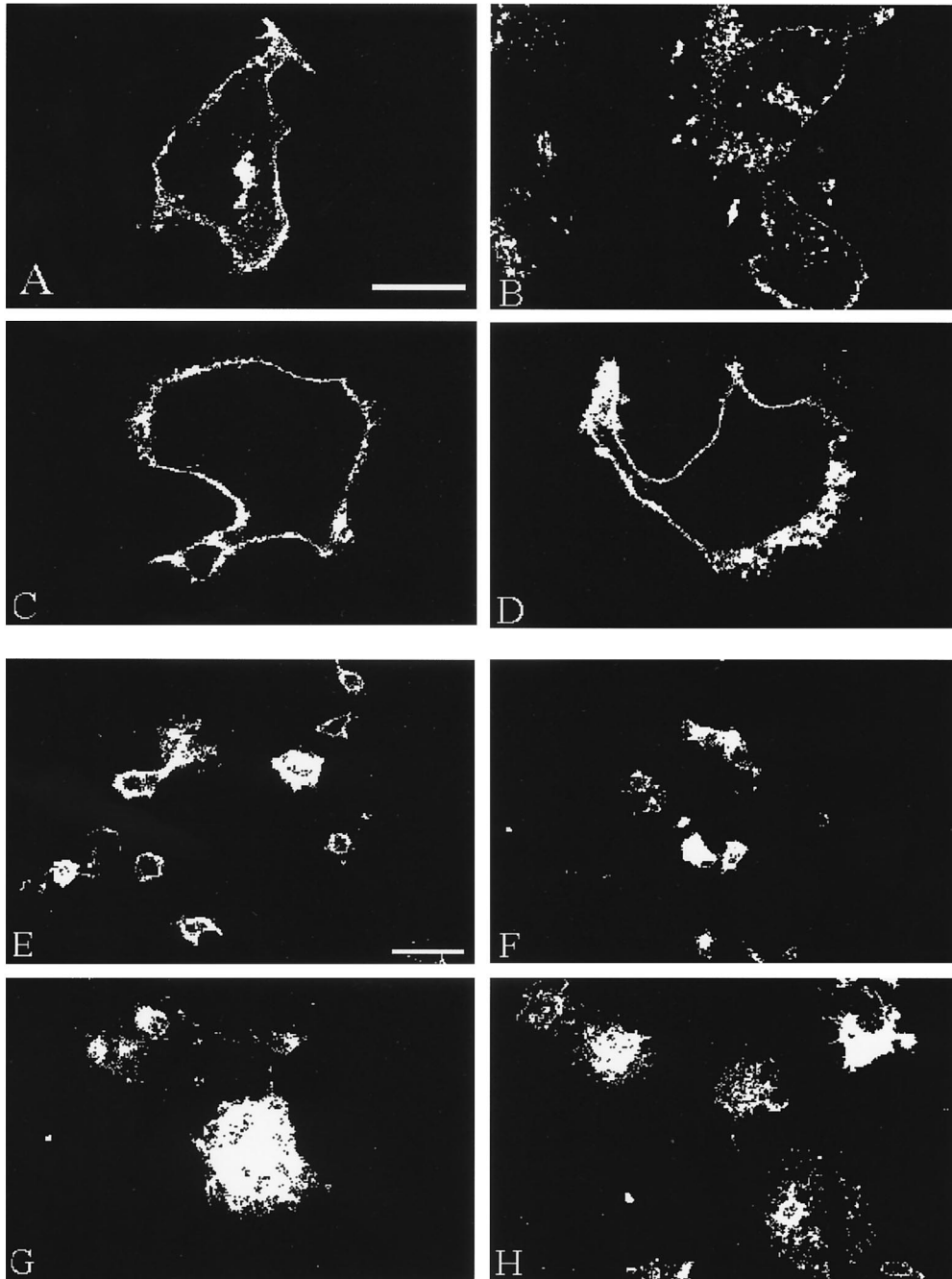


FIG. 1. Confocal microscopy analysis of gH endocytosis and fusion. HeLa cells were infected with VV-T7 then transfected with gH-wt+gL (A and E), gH-bt+gL (B and F), gH-Y835A+gL (C and G), or gH-S830stop+gL (D and H) and then processed for the confocal endocytosis assay for a 60-min time point (A to D) or the standard confocal assay (E to H). VZV gH was immunolabeled with MAb 258 and goat anti-mouse Alexa 488. Fusion samples (E to H) were examined at a low magnification ($\times 20$) to generate landscape images. The bar in panel A is $25 \mu\text{m}$ and applies to panels A to D; the bar in panel E is $50 \mu\text{m}$ and applies to panels E to H.

ages. When coexpressed with gL, gH-wt and gH-bt induced the formation of syncytia (Fig. 1E and F, respectively) that were visually smaller than those observed with the endocytosis-deficient gH mutants gH-Y835A and gH-S830stop (Fig. 1G and H, respectively).

To determine whether the sizes of syncytia found in the gH-wt+gL and gH-bt+gL constructs differed significantly from those found in the gH-Y835A+gL and gH-S830stop+gL

samples, we analyzed the individual syncytium sizes with the point counting method (41), measuring syncytia from $\times 20$ magnification micrographs, similar to those images shown in Fig. 1E to H. Expression of gH-wt+gL resulted in syncytia with a median area of $1,350 \mu\text{m}^2$, whereas gH-bt+gL induced syncytia with a median size of $1,575 \mu\text{m}^2$. In contrast, gH-Y835A+gL or gH-S830stop+gL resulted in syncytia with median sizes of $2,250$ or $2,025 \mu\text{m}^2$, respectively. However, the

TABLE 2. Determination of cumulative proportions per rank of syncytia in VZV gH+gL-transfected cells^a

Range	VZV gH-wt+gL			VZV gH-bt+gL			VZV gH-Y835A+gL			VZV gH-S830stop+gL		
	Tally	Cumulative	C proportion	Tally	Cumulative	C proportion	Tally	Cumulative	C proportion	Tally	Cumulative	C proportion
4-<5	3	3	3.2	2	2	2.2	0	0	0	0	0	0
5-<6	29	32	34.8	14	16	17.4	0	0	0	2	2	2.2
6-<7	24	56	60.9	31	47	51	11	11	11.3	11	13	14
7-<8	12	68	73.9	20	67	72.8	15	26	26.8	16	29	31.2
8-<9	13	81	88	16	83	90.2	15	41	42.3	16	45	48.4
9-<10	9	90	97.8	8	91	98.9	12	53	54.6	13	58	62.4
10-<11	2	92	100	1	92	100	11	64	66	12	70	75.3
11-<12	0			0			14	78	80.4	9	79	84.9
12-<13							5	83	85.6	4	83	89.2
13-<14							5	88	90.7	9	92	98.9
14-<15							3	91	93.8	1	93	100
15-<16							2	93	95.9	0		
16-<17							2	95	97.9			
17-<18							0	95	97.9			
18-<19							1	96	99			
19-<20							1	97	100			
20-<21							0					

^a The range column specifies the user-defined ranges of point values used to rank syncytia based on size, with the “4-<5” range being interpreted as “at least 4 points in size but less than 5.” Tally indicates the number of syncytia that fell within the specified range. The cumulative column indicates the cumulative number of syncytia at each rank value. The C proportion (cumulative proportion) column gives the cumulative percentage of syncytia that fell into each rank value.

data had a very wide range due to the heterogeneous sizes of syncytia within each sample (for example, Fig. 1H). As previously shown (41), this aberrant distribution pattern is not amendable to standard statistical analysis based on determination of averages or means.

Measurement of gH+gL fusion by the Kolmogorov-Smirnov statistical test. We selected the Kolmogorov-Smirnov test for fusion analysis, because this methodology can analyze two data sets, without any assumption about the distribution of data within each set (41). To begin a Kolmogorov-Smirnov analysis of the gH fusion data, the point counting data were sorted into size ranks. As displayed in Table 2, the rank values ranged from 4 to <5 to 19 to <20 for the gH+gL data (range column). Also evident from Table 2 was the distribution of data obtained from point counting of the gH+gL samples. For example, 100% of the gH-wt+gL syncytia were 10 points (2,250 μm²) or less, whereas, in contrast, only 66% of the gH-Y835A+gL were 10 points in size or less.

From the calculations in Table 2, the maximum absolute difference (*D*_{max}) was determined (Table 3) by comparing the cumulative proportions between each sample at each rank as listed in Table 2. *D*_{max} was the greatest difference between two

samples (values in boldface in Table 3). For example, the gH-wt+gL sample differed the most from the gH-Y835A+gL sample (wt v Y835A) at a rank of 6 to <7, with a *D*_{max} of 49.6. Determination of statistical relevance was calculated by using the equation $\lambda = D(mn/m + n)^{1/2}$ as described in Materials and Methods. The calculations for λ and *Q* are listed in Table 3 to illustrate the method of calculation. The analysis documented that the syncytia induced by coexpression of gH-wt+gL were statistically different (*P* < 0.0001) from those induced by either gH-Y835A+gL or gH-S830stop+gL. Similarly, gH-bt+gL syncytia were also significantly different from either gH-Y835A+gL or gH-S830stop+gL (*P* < 0.0001). In contrast, syncytia induced by the two endocytosis mutants, gH-Y835A+gL to gH-S830stop+gL, which exhibited increased levels of fusion (Fig. 1) were not significantly different in size from each other (*P* < 1.0000). Further, comparison of gH-wt+gL to gH-bt+gL also revealed an insignificant difference in the size of syncytia (*P* < 0.1235).

The results from the Kolmogorov-Smirnov test (Tables 2 and 3) are presented graphically in Fig. 2, in a plot with the cumulative percentage of syncytia (*y* axis) that fell within a specific range of point values (*x* axis). The sizes of syncytia

TABLE 3. Kolmogorov-Smirnov calculations for determination of *D*_{max} and *P* values for syncytia in VZV gH+gL-transfected cells^a

Cell type ^b	Range											λ	<i>Q</i>	<i>P</i>	
	4-<5	5-<6	6-<7	7-<8	8-<9	9-<10	10-<11	11-<12	12-<13	13-<14	14-<15				
wt v bt	1	17.4	9.9	1.1	2.2	1.1	0						1.1800	0.8765	<0.1235
wt v Y835A	3.2	34.8	49.6	47.1	45.7	43.2	34						3.4082	1.0000	<0.0001
wt v S830	3.2	32.6	46.9	42.7	39.6	35.4	24.7						3.1894	1.0000	<0.0001
Y835A v bt	2.2	17.4	39.7	46	47.9	44.3	34						3.2914	1.0000	<0.0001
S830 v bt	2.2	15.2	37	41.6	41.8	36.5	24.7						2.8427	1.0000	<0.0001
Y835A v S830	0	2.2	2.7	4.4	6.1	7.8	9.3	4.5	3.6	8.2	6.2		0.0641	0.0000	<1.0000

^a The *D*_{max} value for each set of compared samples is shown in boldface. This value was used for the calculation of *Q*. λ was calculated from $\lambda = D(mn/m + n)^{1/2}$, where *m* and *n* are the population sizes of each sample, as detailed in the text. *Q* was derived by input of λ into table from Hollander and Wolfe (23). The *P* value was derived by subtraction of *Q* from 1 (value = 1 - *Q*). *P* values of <0.05 are significant.

^b v, versus.

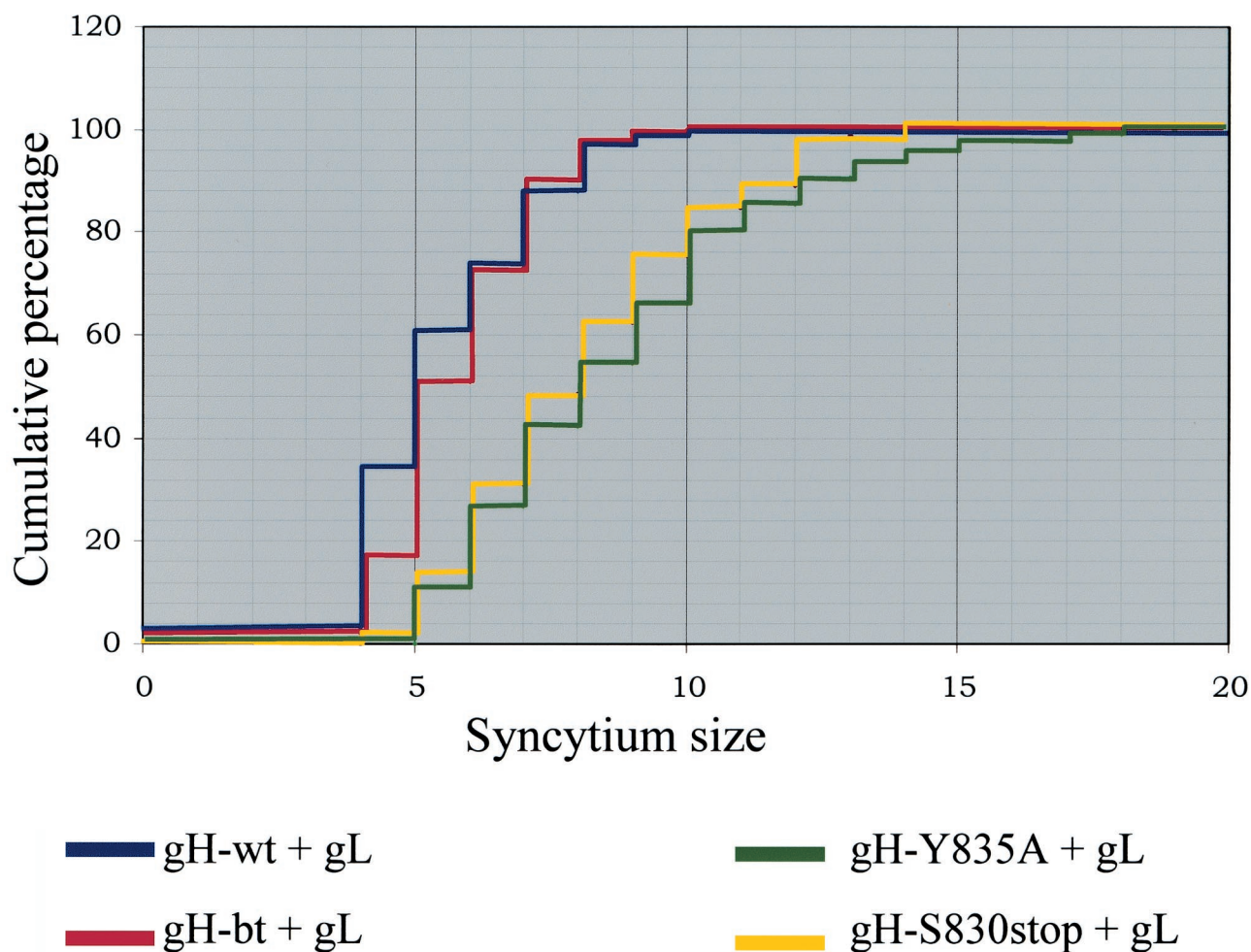


FIG. 2. Graphical representation of gH+gL-mediated fusion with the Kolmogorov-Smirnov statistical test. The data from Tables 2 and 3 were plotted, with the syncytia size range on the *x* axis, and the cumulative percentage on the *y* axis. The results for gH-wt+gL are represented by the blue line, the results for gH-bt+gL are represented by the red line, the results for gH-Y835A+gL are represented by the green line, and the results for gH-S830stop+gL are represented by the yellow line.

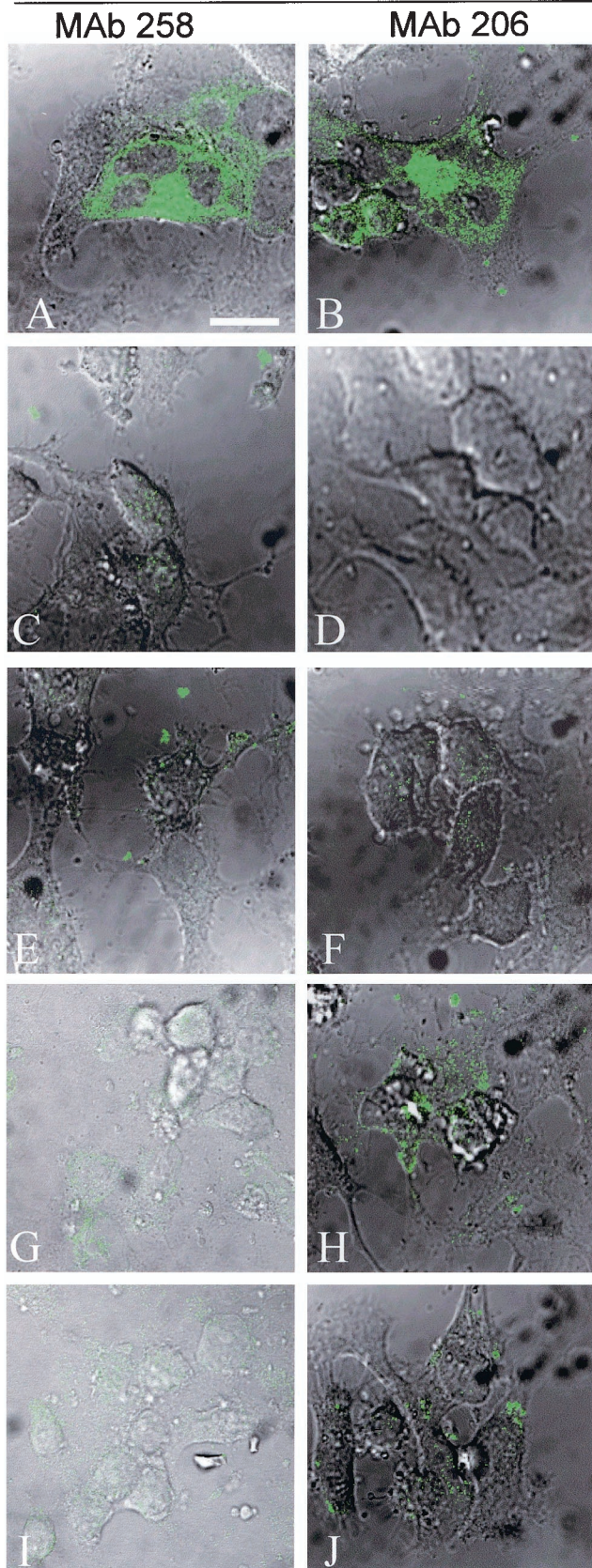
induced in the gH-wt+gL sample (blue line) and the gH-bt+gL (red line) both visibly differed from that of the gH-Y835A+gL (green line) and gH-S830stop+gL (yellow line). In contrast, the gH-wt+gL sample did not differ from the gH-bt+gL sample, as shown by the overlapping plots for these two samples. Thus, we were able to categorize the four gH constructs into two groups: endocytosis competent with less fusion and endocytosis deficient with increased fusion.

Analysis of gH and gH+gE cytoplasmic expression. In the absence of the gL protein, wild-type gH is unable to traffic to the surface or induce fusion (10, 11). However, in transfection studies, gH-bt can travel to the plasma membrane by itself, where it forms patches containing a nonfusogenic form of gH (10). In another set of transfection experiments, we previously demonstrated that gE could partially replace the gL chaperone function and facilitate the transport of gH through the endo-

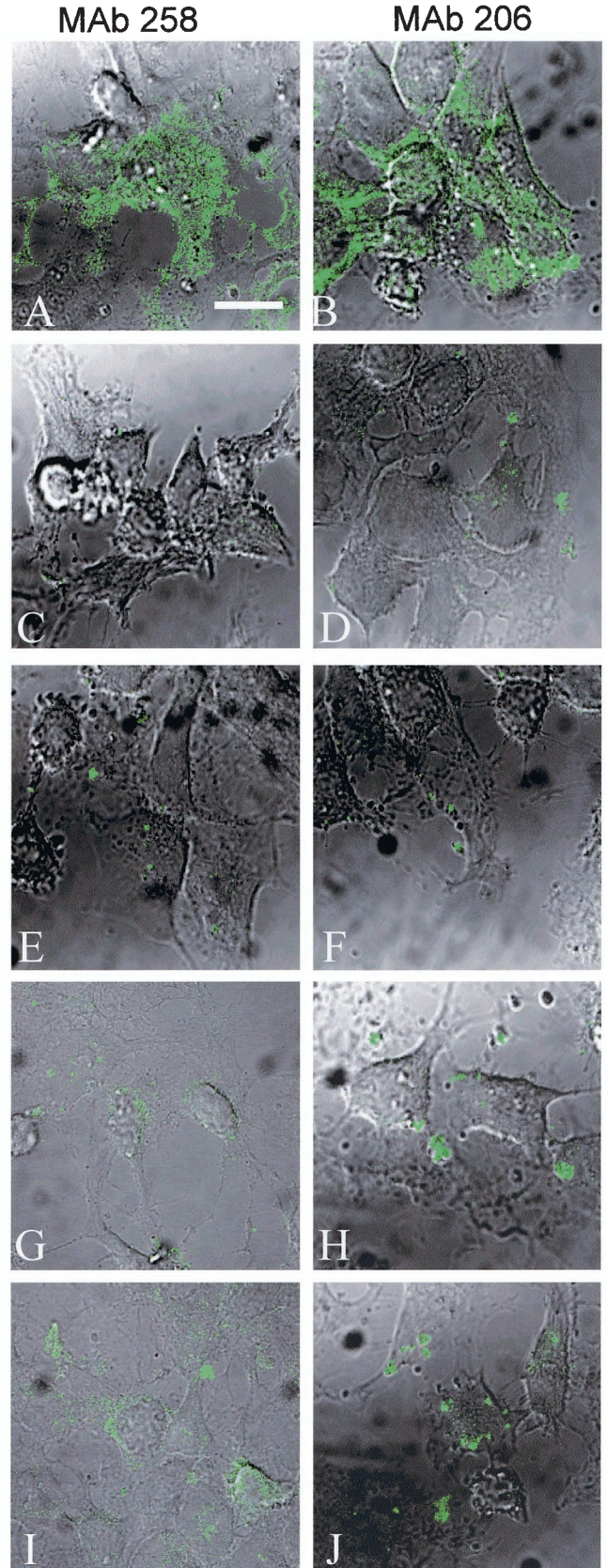
FIG. 3. Cytoplasmic expression of immature and mature gH when expressed alone or with gE. HeLa cells were infected with VV-T7 and then transfected with gH-wt+gL (A and B), gH-wt (C and D), gH-Y835A (E and F), gH-wt+gE (G and H), or gH-Y835A+gE (I and J) and processed for the standard confocal assay. Samples were fixed with permeabilization to label cytoplasmic glycoproteins. Samples were incubated with MAb 258 (A, C, E, G, and I) or MAb 206 (B, D, F, H, and J), followed by goat anti-mouse Alexa 488 (green). Images were collected with both the fluorescent channel and by Nomarski imaging to show cell morphology. The bar in panel A is 25 μ m.

FIG. 4. Surface expression of immature and mature gH when expressed alone or with gE. HeLa cells were infected with VV-T7 then transfected with gH-wt + gL (A and B), gH-wt (C and D), gH-Y835A (E and F), gH-wt + gE (G and H), or gH-Y835A + gE (I and J) and processed for the standard confocal assay. Samples were fixed without permeabilization to label only surface glycoproteins. Samples were incubated with MAb 258 (A, C, E, G, and I) or MAb 206 (B, D, F, H, and J), followed by goat-anti-mouse Alexa 488. Images were collected with both the fluorescent channel and by Nomarski imaging to show cell morphology. The bar in panel A is 25 μ m.

3 Cytoplasmic gH



4 Cell surface gH



plasmic reticulum-Golgi (ER/Golgi). However, fully mature gH is never formed; instead, patches of gH appear on the cell surface (11).

To determine whether the gH endocytosis mutants were endowed with gL-independent properties induced by cytoplasmic tail mutations, an immunolabeling analysis was performed on transfected HeLa cells expressing gH-wt+gL (Fig. 3A and B), gH-wt (Fig. 3C and D), and gH-Y835A (Fig. 3E and F). In addition, the effect of gE coexpression was similarly tested on transfected cells expressing gH-wt+gE (Fig. 3G and H) or gH-Y835A+gE (Fig. 3I and J). VZV gH expression of gH-bt, gH-bt+gE, gH-S830stop, and gH-S830stop+gE were tested as well (data not shown). The cells were permeabilized and labeled with MAb 258 for detection of immature gH (Fig. 3A, C, E, G, and I) or with MAb 206 to detect mature gH (Fig. 3B, D, F, H, and J).

When coexpressed with gL, gH-wt was found throughout the cytoplasm with both MAb 258 and MAb 206 (Fig. 3A and B, respectively). Furthermore, gH+gL induced the formation of syncytia. In contrast, in the absence of gL, the levels of cytoplasmic expression of gH-wt detected with MAb 258 or MAb 206 (Fig. 3C and D) was negligible, i.e., indistinguishable from untransfected controls (data not shown). Similar results were found with gH-Y835A (Fig. 3E and F) and gH-S830stop (data not shown). In addition, no fusion was observed in any gH samples lacking gL. These results indicated that the mutations in the cytoplasmic tail did not confer upon gH the ability to transit the ER/Golgi in the absence of gL.

When gH-wt+gE-cotransfected cells were assayed for cytoplasmic gH production, very low levels of an immature gH form were found in the cytoplasm (Fig. 3G). When tested with MAb 206, gH in the gH-wt+gE sample was detected in patches at the cell surface (Fig. 3H). The results with endocytosis mutants gH-Y835A and gH-S830stop+gE were similar to gH-wt+gE, in that low amounts of cytoplasmic gH were detected (Fig. 3I and data not shown), along with patches on the surface (Fig. 3J and data not shown). Thus, coexpression of gE with any of the four gH constructs led to the production of low levels of intracellular immature gH and patches of nonfusogenic gH at the plasma membrane.

Analysis of gH and gH+gE surface expression. We continued our analysis by testing the surface expression of the gH endocytosis mutants in a manner similar to that performed in Fig. 3. As a positive control, examples of gH surface expression and syncytial formation of gH-wt+gL are shown in Fig. 4A and B. When expressed without gL, the gH-wt protein did not reach the surface (Fig. 4C and D), i.e., staining levels were similar to that found with untransfected controls (data not shown). Similarly, in the absence of gL, gH-Y835A (Fig. 4E and F) and gH-S830stop (data not shown) were not detectable at the surface. When gH-wt+gE surface expression was tested in unpermeabilized cells with MAb 258, the signal for immature gH was barely detectable at the cell surface (Fig. 4G). Labeling of similarly transfected monolayers also revealed little to no mature gH, as defined by MAb 206 labeling, at the cell surface, with most of the fluorescent signal involved in patches or caps (Fig. 4H). Labeling with MAb 258 produced similar results with gH-Y835A+gE (Fig. 4I) and gH-S830stop+gE (data not shown). Also, patches were observed when the endocytosis mutant was coexpressed with gE and tested with

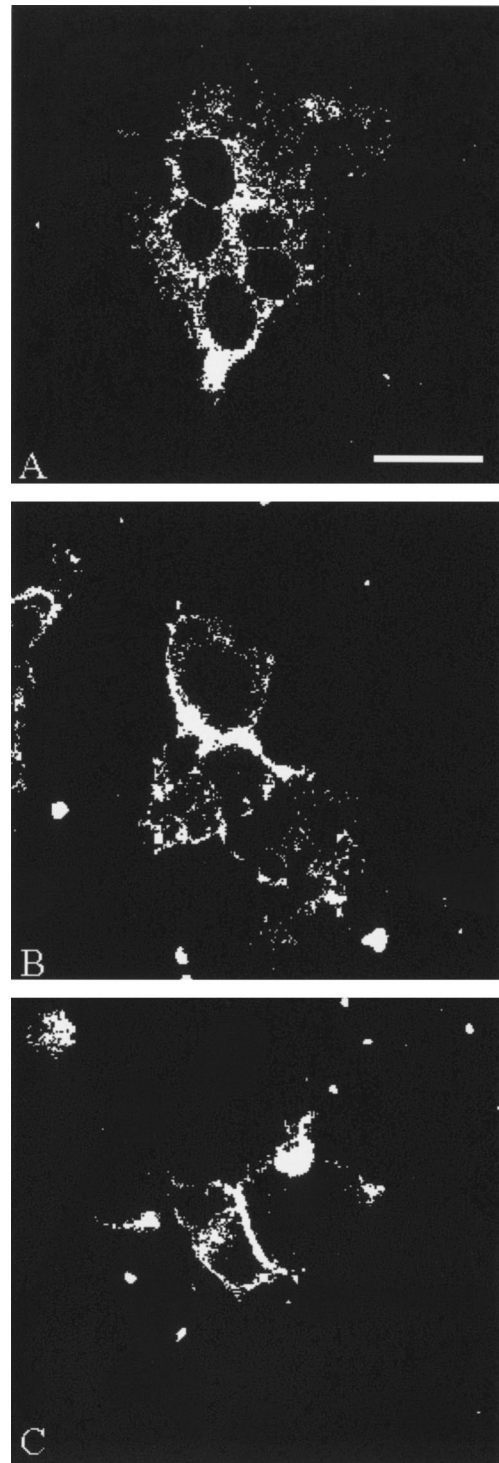


FIG. 5. Antibody-mediated inhibition of fusion. HeLa cells were infected with VV-T7 and then transfected with gH-Y835A+gL (A and B) or gH-S830stop+gL (C). At 4 h posttransfection, 40 μ l of MAb 206 was added for overnight incubation at 37°C (B and C only). At 18 h posttransfection, samples were processed for the steady-state confocal assay with MAb 258 and goat anti-mouse Alexa 488 to detect gH+gL-transfected cells. The bar in panel A is 25 μ m.

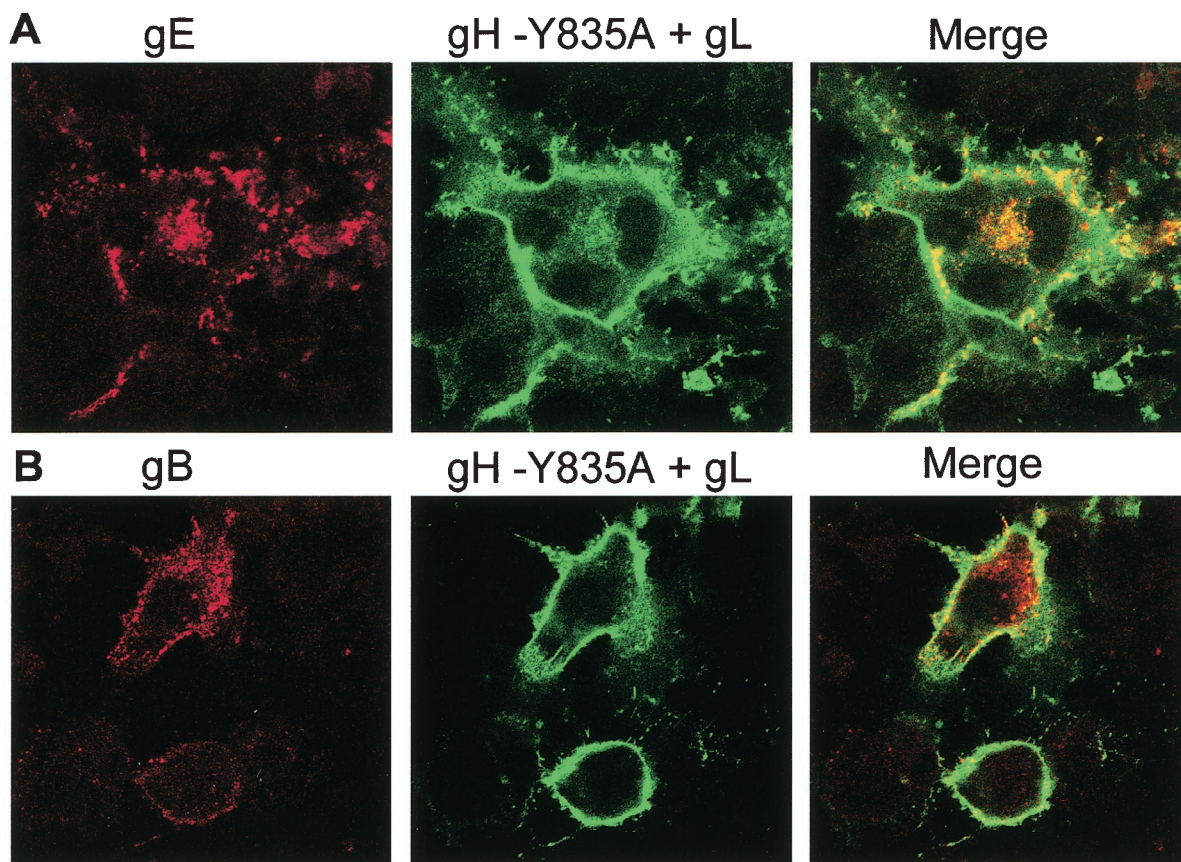


FIG. 6. Coendocytosis of VZV gH-Y835A by gE but not gB. HeLa cells were infected with VV-T7 and then transfected as specified and processed for a 60-min endocytosis time point. (A) Cells transfected with gH-Y835A, gE, and gL and then labeled with murine MAb 3B3 for gE (red) and human MAb V3 for gH (green). (B) Cells transfected with gH-Y835A, gB, and gL, and labeled with murine MAb 158 for gB (red) and MAb V3 for gH (green). A merge of the red and green channels is shown in the rightmost panels.

MAb 206 (Fig. 4J). When taken together, these results indicated that the mutations induced in the cytoplasmic tail sequences of gH-Y835A and gH-S830stop did not bestow any new trafficking properties upon the mutants compared to gH-wt.

Of note, the patches of gH on the cell surface were recognized by MAb 206, which binds an epitope on the mature and fusogenic form of gH, yet no fusion was observed in the gH-wt+gE-transfected cells. This result suggested that the form of gH in the patches, although still not fully mature, contains a partially recognizable B-cell epitope. This conclusion is reasonable since an MAb may recognize an incomplete conformational B-cell epitope, albeit with lower affinity.

Antibody-mediated inhibition of gH+gL cell-to-cell fusion. MAb 206 inhibits cell-to-cell fusion in gH+gL-transfected cells (11). To ensure that the mutations induced in the cytoplasmic tails of gH-Y835A and gH-S830stop did not result in the formation of a novel fusogenic domain or otherwise alter the structure of gH so as to increase its fusogenicity, we tested whether or not overnight incubation with MAb 206 inhibited fusion mediated by the gH endocytosis-deficient proteins. In the absence of MAb 206, gH-Y835A+gL induced the formation of syncytia (Fig. 5A). In contrast, when MAb 206 was added to gH-Y835A+gL-transfected cells (Fig. 5B), cell-to-cell fusion was blocked, and only single cells were found.

Shown in Fig. 5B are two directly adjacent cotransfected cells, between which the intact plasma membrane was still visible. Similar results were observed with gH-S830stop+gL transfected cells treated with MAb 206 overnight (Fig. 5C). In data not shown, the addition of the anti-gE MAb 3B3 as a control demonstrated no inhibitory effect on cell-to-cell fusion.

Endocytosis of gH-Y835A when coexpressed with gE or gB. VZV gE contains a functional YAGL endocytosis motif in its cytoplasmic tail (40). We next sought to determine whether complex formation between gE and an endocytosis-deficient form of gH would lead to gH endocytosis. As a control experiment, we performed a cotransfection experiment with mutated gH and wild-type gB. VZV gB undergoes endocytosis via tyrosine-based motifs (22) but is not known to interact with gH.

Internalization of gH-Y835A when coexpressed with gE and gL was examined after 60 min of endocytosis (Fig. 6A). Internalized gE was readily apparent after 60 min of endocytosis. In contrast to the negative results obtained with gH-Y835A+gL (Fig. 1C), gH endocytosis was observed when this mutant was coexpressed with both gL and gE. Merging of the red and green channels formed a yellow signal, a result which suggested that complex formation between gE and an endocytosis-deficient form of gH occurred at the plasma membrane and led to coendocytosis of the two glycoproteins. In contrast to the results with gE, coexpression of gB with gH-Y835A+gL did not

lead to endocytosis of gH, since gB was found in the cytoplasm in substantial amounts, whereas gH-Y835A was hardly detected (Fig. 6B). The faint yellow signal may represent bulk membrane transport of small amounts of gH. Taken together, these results documented the specificity of the mutant gH:gE endocytosis event.

To further document the above interaction between VZV gE and gH, we tested whether precipitation of gH would coprecipitate gE from infected cells. This experiment was carried out first with mouse antibody reagents and then repeated with human MAb to gH. As shown in Fig. 7, under both conditions a gE protein coprecipitated by a gH antibody was detected by a gE antibody. When only murine reagents were used, the heavy and light chains of mouse immunoglobulin G antibody also were detected, as expected (Fig. 7A). These two bands were removable by stripping the membrane (Fig. 7B). As a specificity control, we precipitated gB with a human MAb and immunoblotted with a mouse antibody to gH, but no gH band was detected (Fig. 7C). The radioimmune precipitation profiles of the mouse and human antibody reagents to gH are shown as additional controls (Fig. 7D), since these results have not previously been published under the experimental conditions used in the present study. One important negative control (lane 4) showed that anti-gH antibody did not precipitate gE in the absence of gH:gE proteins.

Statistical analysis of cell-to-cell fusion mediated by gH when coexpressed with gL and gE. The extent to which complex formation and coendocytosis of gH and gE at the plasma membrane were affecting the levels of gH-mediated fusion was assessed by repeating the syncytium-measuring assays, with HeLa cells transfected with gL and gE along with gH-wt, gH-bt, gH-Y835A, or gH-S830stop. The samples were labeled with the anti-gE MAb 3B3 and the anti-gH MAb V3, along with the appropriate fluorophores. Only syncytia expressing both gH and gE were included in the point counting assay and the Kolmogorov-Smirnov analysis.

We first averaged our results in order to directly compare them to our initial gH+gL results. Remarkably, the average sizes for all four transfection conditions were similar. For gH-wt+gL+gE, the average syncytium size was 1,440 μm^2 , whereas for gH-bt+gL+gE the average was 1,462 μm^2 . These results were similar to those obtained for gH-wt+gL and gH-bt+gL. However, for gH-Y8345A+gL+gE and gH-S830stop+gL+gE, the average sizes were 1,440 and 1,395 μm^2 , respectively. The average syncytial sizes for the gH endocytosis mutants were markedly smaller than seen in the previous measurements. Analysis of the fusion data with the Kolmogorov-Smirnov test revealed that the sizes of syncytia induced under each of the four transfection conditions were similar. For each comparison, the *P* value obtained exceeded 0.05, which indicated that no one sample was significantly different from another (Fig. 8).

Cell surface expression of gH in gH +gL-transfected cells. The simplest explanation for the increased fusion in cultures transfected with the gH endocytosis mutants was that endocytosis reduced the levels of gH cell surface expression. To determine whether the endocytosis-deficient but fusogenic gH mutants increased cell-to-cell fusion through increased surface density of gH, surface gH was biotinylated, immunoprecipitated, and then detected with streptavidin-HRP. When tested

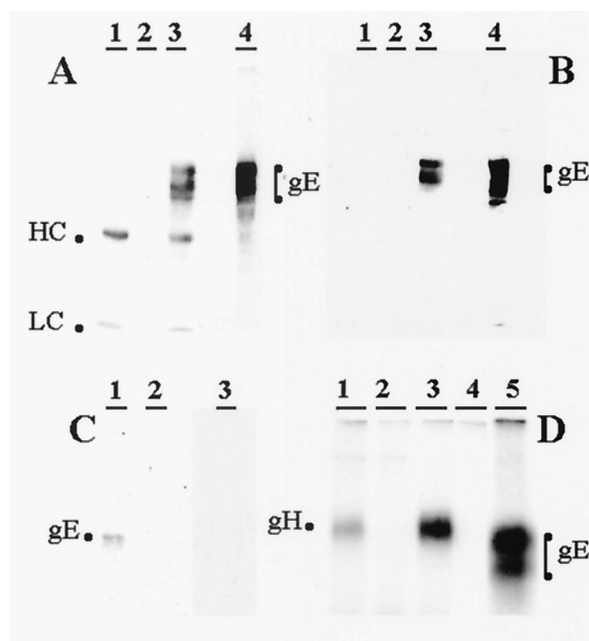


FIG. 7. Immunoprecipitation and immunoblotting of VZV glycoproteins. (A) Precipitation with murine antibodies. VZV-infected cell lysate was either immunoprecipitated with mouse anti-gH MAb (lane 3) or directly subjected to SDS-PAGE (lane 4). Mock-infected cell lysate immunoprecipitated with mouse anti-gH MAb (lane 1) and VZV-infected cell lysate without a MAB immunoprecipitation step (lane 2) were controls. Immunoprecipitates and cell lysate were subjected to SDS-PAGE (8%) under reducing conditions; proteins were electrotransferred to nitrocellulose membrane and probed with mouse anti-gE MAb. The heavy and light chains of the mouse antibody are labeled HC and LC, respectively. (B) Reprobing of the blot in panel A. Nitrocellulose membrane from panel A was stripped and probed for a second time with biotinylated mouse anti-gE MAb and streptavidin-HRP. (C) Precipitation with human antibodies. VZV-infected (lanes 1 and 3) or mock-infected (lane 2) cell lysates were immunoprecipitated with human anti-gH MAb (lanes 1 and 2) and human anti-gB MAb (lane 3). Immunoprecipitates were subjected to SDS-PAGE; proteins were electrotransferred to nitrocellulose membrane and probed with anti-gE MAb (lanes 1 and 2) or mouse anti-gH MAb (lane 3). (D) Radioimmuno-precipitation profiles of VZV gH and gE. HeLa cell cultures were transfected with either plasmids pTM1-gH+pTM1-gL (lanes 1 and 3), pTM1-gE (lane 4 and 5) or mock (lane 2); cultures were labeled with [^{35}S]cysteine-methionine. Cell lysates were immunoprecipitated with Bidesign mouse anti-gH MAb (lanes 1, 2, and 4), human anti-gH MAb (lane 3), and mouse anti-gE MAb (lane 5). Immunoprecipitation and immunoblotting were carried out by previously described methods (10, 17).

in this manner, the size and intensity of the band representing gH-wt+gL (Fig. 9, lane 1) was visibly less than those bands observed for gH-Y835A+gL (Fig. 9, lane 3) and gH-Y830stop+gL (Fig. 9, lane 4). Thus, when immunoprecipitated with MAb V3, we detected increased levels of surface expression with the gH endocytosis mutants.

It was noted that the band representing gH-bt+gL was less intense than that observed for gH-wt+gL (lane 2). However, when the immunoprecipitation experiments were repeated with an epitope-tagged gL (gL.13.3B3) and anti-tag antibody, the result showed that the amount of precipitated gH-bt (as part of a gH:gE complex) was equivalent to gH-wt (data not shown). Thus, the diminished level of gH-bt was likely due to an incompletely formed gH conformational epitope. Subse-

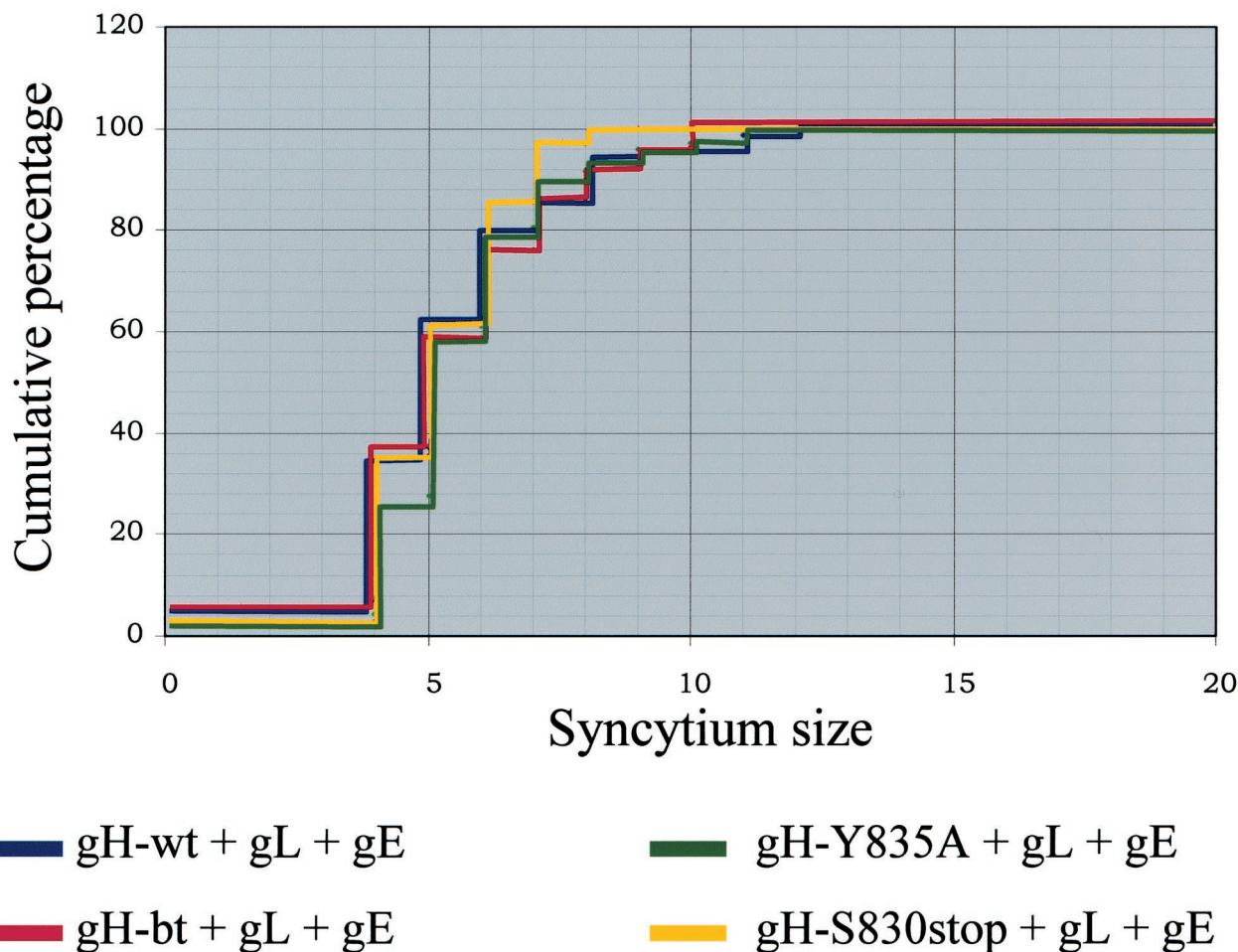


FIG. 8. Graphical representation of gH+gL+gE mediated fusion with the Kolmogorov-Smirnov statistical test. The data were plotted with the syncytium size range on the x axis and the cumulative percentage on the y axis. The results for gH-wt+gL+gE are represented by the blue line, the results for gH-bt+gL+gE are represented by the red line, the results for gH-Y835A+gL+gE are represented by the green line, and the results for gH-S830stop+gL+gE are represented by the yellow line.

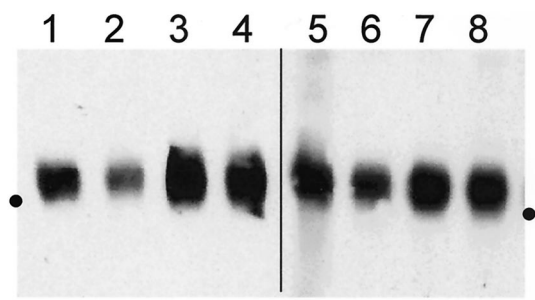
quently, the films generated from the assay were photographed over a light box; the bands were measured for intensity. The endocytosis-deficient forms of gH (Fig. 9, lanes 3 and 4) had increased levels of intensity compared to the endocytosis-competent forms of gH (Fig. 9, lanes 1 and 2), a finding consistent with a visual evaluation of the bands.

Cell surface expression of gH in gH+gL+gE-transfected cells. The degree to which coexpression of gE with the gH endocytosis mutants tempered the levels of cell-to-cell fusion was next assessed. To this end, we repeated the surface biotinylation assay in HeLa cells transfected with the four forms of gH, along with gL and gE; biotinylated cell surface gH was immunoprecipitated with MAb V3. When examined visually, coexpression of gE with gH+gL resulted in similar levels of gH surface expression for gH-wt+gL+gE (Fig. 9, lane 5), gH-Y835A+gL+gE (lane 7), and gH-S830stop+gL+gE (lane 8). As was found previously, the band for gH in the gH-bt+gL+gE sample (lane 6) was again visually lower in intensity. When the four bands were measured with the Kodak 1D system, the intensities of the gH-wt, gH-Y835A, and gH-S830 stop samples were very similar, in accordance with the visual impression.

DISCUSSION

Based on the quantitative VZV fusion assay data acquired through highly statistically significant Kolmogorov-Smirnov analyses, a role for VZV gH endocytosis is proposed. The increased levels of fusion observed in the gH-Y835A+gL and gH-S830stop+gL transfected cells were markedly greater than the levels observed in gH-wt+gL or gH-bt+gL samples. The latter group was endocytosis competent and displayed wild-type levels of cell-to-cell fusion. The former group, which included the two mutants gH-Y835A and gH-S830stop, was endocytosis deficient and exhibited increased levels of fusion. The former group also exhibited increased amounts of surface gH. Therefore, we conclude that gH endocytosis leads to decreased cell-to-cell fusion in association with decreased surface density of gH.

Endocytosis and fusion in different viral systems. Endocytosis is now recognized as a property of structural glycoproteins in several viral systems. The transmembrane (TM) protein of the retroviral Env complex contains a functional tyrosine-based endocytosis motif that facilitates internalization via clathrin-



Lane	Sample	Intensity
1	gH-wt + gL	140
2	gH-bt + gL	104
3	gH-Y835A + gL	188
4	gH-S830stop + gL	166
5	gH-wt + gL + gE	168
6	gH-bt + gL + gE	155
7	gH-Y835A + gL + gE	169
8	gH-S830stop + gL + gE	167

Closed circles in margins indicate 97 kd

FIG. 9. Cell surface expression of gH in gH+gL- and gH+gL+gE-transfected cells. HeLa cells were infected with VV-T7 and then transfected with gH-wt+gL (lane 1), gH-bt+gL (lane 2), gH-Y835A+gL (lane 3), or gH-S830stop+gL (lane 4) and processed for the surface biotinylation assay. Alternatively, HeLa cells were transfected with gH-wt+gL+gE (lane 5), gH-bt+gL+gE (lane 6), gH-Y835A+gL+gE (lane 7), or gH-S830stop+gL+gE (lane 8). For each lane, one 35-mm well was immunoprecipitated with 1 μ l of Mab V3. Samples were resolved in an 8% PAGE gel under nonreducing conditions. Lanes 1 to 4 and lanes 5 to 8 represent two separate experiments. The intensity of each band was determined with the Kodak 1D software. The program defined the perimeter of the bands, and measured the mean intensity. The values are listed in the bottom half of the figure.

coated pits. A tyrosine-to-cysteine mutation (Y723C) in the tyrosine based motif of the simian immunodeficiency virus (SIV) TM protein blocks endocytosis of the protein (46). In turn, removal of the endocytosis signal in the SIV transmembrane domain increases cell-to-cell fusion and accelerates the kinetics of viral spread through increased surface expression (27, 46). Similar motifs in related retroviral TM proteins regulate cell surface expression of the protein via endocytosis (3, 4, 9, 46).

Likewise, resistance of cell lines to human T-cell leukemia virus type 1 syncytium formation is overcome by truncation of the human T-cell leukemia virus TM glycoprotein by eight amino acids (25). Interestingly, the truncation interrupts a tyrosine-based endocytosis motif near the C terminus of the TM cytoplasmic tail. In studies with equine infectious anemia virus, a novel cytolitic strain has been described recently, which also has enhanced spread and fusion properties (31). When the proviral genome was sequenced, a stop codon was detected in the Env gene. This mutation would result in a glycoprotein with a complete ectodomain and transmembrane domain but a

markedly shortened endodomain. In addition to the retroviruses, another example of a possible relationship between fusion and glycoprotein trafficking is found in the measles virus (33).

Finally, endocytosis and fusion has been investigated in HSV containing mutated forms of gB (12). HSV gB contains one dileucine- and two tyrosine-based endocytosis motifs. Numerous HSV *syn* mutations are localized to the C-terminal domain of gB (2, 5, 14, 37, 49). Removal of the C-terminal tyrosine motif of HSV-2 gB (867-YSP-870) by truncation confers a syncytial phenotype with no effect on virus-to-cell fusion during entry (12). With regard to VZV gB, the dileucine motif in VZV gB (841-LL-842) is not required for endocytosis, whereas the C-terminal tyrosine based motif (857-YSRV-860) is most critical (22). Further obfuscating the matter, truncation of VZV gB by 36 amino acids in a VZV recombinant virus induces the formation of extensive syncytia, whereas the mutant gB still undergoes endocytosis via a third tyrosine-based endocytosis motif (818-YMTL-821) (21). To summarize, because of the complexity of their three endocytosis motifs, more detailed investigations of trafficking with mutated gB proteins (HSV or VZV) are required in order to determine the precise relationship of gB endocytosis to cell surface expression and cell-to-cell fusion.

Other amino acid residues involved in fusion. Both HSV-1 and HSV-2 gH lack any known endocytosis motif in their endodomain (42). However, other amino acids in the cytoplasmic tail and transmembrane domain of HSV-1 gH have been implicated in cell-to-cell fusion (51). Specifically, mutagenesis studies of a serine-valine-proline sequence in the HSV-1 tail indicate a role for this tripeptide in cell-to-cell fusion. Deletion of this motif in HSV recombinant viruses results in decreased entry and syncytium formation (51).

A second HSV-1 study has revealed a transmembrane domain glycine residue that is critical for fusion function and is common to alphaherpesvirus gH homologues (18). A fusion role for this intramembrane glycine was first demonstrated in the vesicular stomatitis virus G glycoprotein and the influenza virus hemagglutinin (6, 32). This conserved glycine residue is found in HSV-1, HSV-2, VZV, pseudorabies virus, equine herpesvirus, and bovine herpesvirus. Mutation of a glycine residue (G812) centrally located in the HSV-1 gH transmembrane domain abolishes gH-mediated fusion (18).

Interaction of VZV gE with gH and subsequent fusion. In contrast to other alphaherpesviruses, VZV gE is the predominant viral glycoprotein in infected cells. Although gE is often found in a gE:gI complex, dimers and trimers of gE have also been detected (7, 16). Neither gE nor the gE:gI complex is fusogenic. In cited studies, we demonstrated that gE and gI harbored tyrosine- and dileucine-based internalization motifs, respectively. VZV gE navigates a complicated series of trafficking pathways postendocytosis, which include both recycling to the cell surface and traveling to the trans-Golgi network (24). Phosphorylation of a cluster of serine/threonine residues in the gE cytoplasmic tail by casein kinase II and the ORF47 protein serine kinase (HSV-1 UL13 homologue) determines which pathway is taken (24). In addition, under transfection conditions, complex formation between gE and gI can mediate the internalization of a gI endocytosis mutant (39).

In a similar manner, we have now shown under transfection conditions that gE can form a complex with gH and facilitate

internalization of endocytosis-deficient gH mutant proteins from the cell surface. We previously demonstrated that gE can mediate gL-independent trafficking of an immature gH from the ER/Golgi to the plasma membrane (11). The specificity of the gH+gE interaction during endocytosis was confirmed by cotransfection of gB with the gH-Y835A. In contrast to the gE+gH interaction, little or no endocytosis of gH was observed when it was cotransfected with gB. The latter studies may further expand the properties of VZV gE (16). For example, even though the short cytoplasmic tail of gH is now known to contain a functional endocytosis motif, it does not contain other trafficking motifs found in gE, such as a phosphorylation site or an acidic TGN targeting sequence (24, 53, 55, 56). Therefore, a gE:gH complex (or a gH:gL:gE complex) would likely be shuttled via a different cytoplasmic pathway than the gH:gL complex after internalization. Further experiments will also need to be carried out in the context of a recombinant virus with mutated gE and gH glycoproteins.

ACKNOWLEDGMENTS

T.J.P. thanks the members of her microbiology doctoral thesis committee for helpful advice. C.G. thanks the participants of the 11th International Conference on Immunobiology and Prophylaxis of Human Herpesvirus Infections (Taormina, Italy) for critical comments.

This research was supported by NIH grant AI22795 and a fellowship award from the VZV Research Foundation, New York, N.Y.

REFERENCES

- Avitabile, E., G. Lombardi, and G. Campadelli-Fiume. 2003. Herpes simplex virus glycoprotein K, but not its syncytial allele, inhibits cell-cell fusion mediated by the four fusogenic glycoproteins, gD, gB, gH, and gL. *J. Virol.* **77**:6836–6844.
- Baghian, A., L. Huang, S. Newman, S. Jayachandra, and K. G. Kousoulas. 1993. Truncation of the carboxy-terminal 28 amino acids of glycoprotein B specified by herpes simplex virus type 1 mutant *amb1511-7* causes extensive cell fusion. *J. Virol.* **67**:2396–2401.
- Berlitz-Torrent, C., B. L. Shacklett, L. Erdtmann, L. Delamarre, I. Bouchaert, P. Sonigo, M. C. Dokhelar, and R. Benarous. 1999. Interactions of the cytoplasmic domains of human and simian retroviral transmembrane proteins with components of the clathrin adaptor complexes modulate intracellular and cell surface expression of envelope glycoproteins. *J. Virol.* **73**:1350–1361.
- Bowers, K., A. Pelchen-Matthews, S. Honing, P. J. Vance, L. Creary, B. S. Haggarty, J. Romano, W. Ballensiefen, J. A. Hoxie, and M. Marsh. 2000. The simian immunodeficiency virus envelope glycoprotein contains multiple signals that regulate its cell surface expression and endocytosis. *Traffic* **1**:661–674.
- Cai, W. H., B. Gu, and S. Person. 1988. Role of glycoprotein B of herpes simplex virus type 1 in viral entry and cell fusion. *J. Virol.* **62**:2596–2604.
- Cleverley, D. Z., and J. Lenard. 1998. The transmembrane domain in viral fusion: essential role for a conserved glycine residue in vesicular stomatitis virus G protein. *Proc. Natl. Acad. Sci. USA* **95**:3425–3430.
- Cohen, J. I., and H. Nguyen. 1997. Varicella-zoster virus glycoprotein I is essential for growth of virus in Vero cells. *J. Virol.* **71**:6913–6920.
- Cole, N. L., and C. Grose. 2003. Membrane fusion mediated by herpesvirus glycoproteins: the paradigm of varicella-zoster virus. *Rev. Med. Virol.* **13**:207–222.
- Deschambeault, J., J. P. Lalonde, G. Cervantes-Acosta, R. Lodge, E. A. Cohen, and G. Lemay. 1999. Polarized human immunodeficiency virus budding in lymphocytes involves a tyrosine-based signal and favors cell-to-cell viral transmission. *J. Virol.* **73**:5010–5017.
- Duus, K. M., and C. Grose. 1996. Multiple regulatory effects of varicella-zoster virus (VZV) gL on trafficking patterns and fusogenic properties of VZV gH. *J. Virol.* **70**:8961–8971.
- Duus, K. M., C. Hatfield, and C. Grose. 1995. Cell surface expression and fusion by the varicella-zoster virus gH:gL glycoprotein complex: analysis by laser scanning confocal microscopy. *Virology* **210**:429–440.
- Fan, Z., M. L. Grantham, M. S. Smith, E. S. Anderson, J. A. Cardelli, and M. I. Muggerridge. 2002. Truncation of herpes simplex virus type 2 glycoprotein B increases its cell surface expression and activity in cell-cell fusion, but these properties are unrelated. *J. Virol.* **76**:9271–9283.
- Forghani, B., L. Ni, and C. Grose. 1994. Neutralization epitope of the varicella-zoster virus gH:gL glycoprotein complex. *Virology* **199**:458–462.
- Gage, P. J., M. Levine, and J. C. Glorioso. 1993. Syncytium-inducing mutations localize to two discrete regions within the cytoplasmic domain of herpes simplex virus type 1 glycoprotein B. *J. Virol.* **67**:2191–2201.
- Gershon, A., L. Cosio, and P. A. Brunell. 1973. Observations on the growth of varicella-zoster virus in human diploid cells. *J. Gen. Virol.* **18**:21–31.
- Grose, C. 2002. The predominant varicella-zoster virus gE and gI glycoprotein complex, p. 183–211. *In* E. Bogner and A. Holzenburg (ed.), *Structure function relationships of human pathogenic viruses*. Kluwer Academic Press, London, England.
- Grose, C., D. P. Edwards, W. E. Friedrichs, K. A. Weigle, and W. L. McGuire. 1983. Monoclonal antibodies against three major glycoproteins of varicella-zoster virus. *Infect. Immun.* **40**:381–388.
- Harman, A., H. Browne, and T. Minson. 2002. The transmembrane domain and cytoplasmic tail of herpes simplex virus type 1 glycoprotein H play a role in membrane fusion. *J. Virol.* **76**:10708–10716.
- Harson, R., and C. Grose. 1995. Egress of varicella-zoster virus from the melanoma cell: a tropism for the melanocyte. *J. Virol.* **69**:4994–5010.
- Hatfield, C., K. M. Duus, J. Chen, D. H. Jones, and C. Grose. 1997. Epitope mapping and tagging by recombination PCR mutagenesis. *BioTechniques* **22**:332–337.
- Heineman, T. C., and S. L. Hall. 2002. Role of the varicella-zoster virus gB cytoplasmic domain in gB transport and viral egress. *J. Virol.* **76**:591–599.
- Heineman, T. C., and S. L. Hall. 2001. VZV gB endocytosis and Golgi localization are mediated by YXXL motifs in its cytoplasmic domain. *Virology* **285**:42–49.
- Hollander, M., and D. A. Wolfe. 1973. *Nonparametric statistical methods*. John Wiley & Sons, Inc., New York, N.Y.
- Kenyon, T. K., J. I. Cohen, and C. Grose. 2002. Phosphorylation by the varicella-zoster ORF47 protein serine kinase determines whether endocytosed viral gE traffics to the *trans*-Golgi network or recycles to the cell membrane. *J. Virol.* **76**:10980–10993.
- Kim, F. J., N. Manel, Y. Boublik, J. L. Battini, and M. Sitbon. 2003. Human T-cell leukemia virus type 1 envelope-mediated syncytium formation can be activated in resistant mammalian cell lines by a carboxy-terminal truncation of the envelope cytoplasmic domain. *J. Virol.* **77**:963–969.
- Klupp, B. G., R. Nixdorf, and T. C. Mettenleiter. 2000. Pseudorabies virus glycoprotein M inhibits membrane fusion. *J. Virol.* **74**:6760–6768.
- LaBranche, C. C., M. M. Sauter, B. S. Haggarty, P. J. Vance, J. Romano, T. K. Hart, P. J. Bugelski, and J. A. Hoxie. 1994. Biological, molecular, and structural analysis of a cytopathic variant from a molecularly cloned simian immunodeficiency virus. *J. Virol.* **68**:5509–5522.
- Larsen, J. O. 1998. Stereology of nerve cross sections. *J. Neurosci. Methods* **85**:107–118.
- Maresova, L., T. Pasięka, T. Wagenaar, W. Jackson, and C. Grose. 2003. Identification of the authentic varicella-zoster virus gB (gene 31) initiating methionine overlapping the 3' end of gene 30. *J. Med. Virol.* **70**:S64–S70.
- Maresova, L., T. J. Pasięka, and C. Grose. 2001. Varicella-zoster virus gB and gE coexpression, but not gB or gE alone, leads to abundant fusion and syncytium formation equivalent to those from gH and gL coexpression. *J. Virol.* **75**:9483–9492.
- Maury, W., P. J. Wright, and S. Bradley. 2003. Characterization of a cytolytic strain of equine infectious anemia virus. *J. Virol.* **77**:2385–2399.
- Melikian, G. B., S. Lin, M. G. Roth, and F. S. Cohen. 1999. Amino acid sequence requirements of the transmembrane and cytoplasmic domains of influenza virus hemagglutinin for viable membrane fusion. *Mol. Biol. Cell* **10**:1821–1836.
- Moll, M., H. D. Klenk, G. Herrler, and A. Maisner. 2001. A single amino acid change in the cytoplasmic domains of measles virus glycoproteins H and F alters targeting, endocytosis, and cell fusion in polarized Madin-Darby canine kidney cells. *J. Biol. Chem.* **276**:17887–17894.
- Montalvo, E. A., and C. Grose. 1987. Assembly and processing of the disulfide-linked varicella-zoster virus glycoprotein gpII (gB). *J. Virol.* **61**:2877–2884.
- Montalvo, E. A., and C. Grose. 1986. Neutralization epitope of varicella zoster virus on native viral glycoprotein gp118 (VZV glycoprotein gH). *Virology* **149**:230–241.
- Moss, B., O. Elroy-Stein, T. Mizukami, W. A. Alexander, and T. R. Fuerst. 1990. Product review: new mammalian expression vectors. *Nature* **348**:91–92.
- Muggerridge, M. I. 2000. Characterization of cell-cell fusion mediated by herpes simplex virus 2 glycoproteins gB, gD, gH, and gL in transfected cells. *J. Gen. Virol.* **81**:2017–2027.
- Nyengaard, J. R. 1999. Stereologic methods and their application in kidney research. *J. Am. Soc. Nephrol.* **10**:1100–1123.
- Olson, J. K., and C. Grose. 1998. Complex formation facilitates endocytosis of the varicella-zoster virus gE:gI Fc receptor. *J. Virol.* **72**:1542–1551.
- Olson, J. K., and C. Grose. 1997. Endocytosis and recycling of varicella-zoster virus Fc receptor glycoprotein gE: internalization mediated by a YXXL motif in the cytoplasmic tail. *J. Virol.* **71**:4042–4054.
- Pasięka, T. J., R. F. Woolson, and C. Grose. 2003. Viral induced fusion and syncytium formation: measurement by the Kolmogorov-Smirnov statistical test. *J. Virol. Methods* **111**:157–161.
- Pasięka, T. J., L. Maresova, and C. Grose. 2003. A functional YNKI motif in

- the short cytoplasmic tail of varicella-zoster virus glycoprotein gH mediates clathrin-dependent and antibody-independent endocytosis. *J. Virol.* **77**: 4191–4204.
43. **Pertel, P. E.** 2002. Human herpesvirus 8 glycoprotein B (gB), gH, and gL can mediate cell fusion. *J. Virol.* **76**:4390–4400.
 44. **Rodriguez, J. E., T. Moninger, and C. Grose.** 1993. Entry and egress of varicella virus blocked by same anti-gH monoclonal antibody. *Virology* **196**: 840–844.
 45. **Santos, R. A., J. A. Padilla, C. Hatfield, and C. Grose.** 1998. Antigenic variation of varicella zoster virus Fc receptor gE: loss of a major B-cell epitope in the ectodomain. *Virology* **249**:21–31.
 46. **Sauter, M. M., A. Pelchen-Matthews, R. Bron, M. Marsh, C. C. LaBranche, P. J. Vance, J. Romano, B. S. Haggarty, T. K. Hart, W. M. Lee, and J. A. Hoxie.** 1996. An internalization signal in the simian immunodeficiency virus transmembrane protein cytoplasmic domain modulates expression of envelope glycoproteins on the cell surface. *J. Cell Biol.* **132**:795–811.
 47. **Sugano, T., T. Tomiyama, Y. Matsumoto, S. Sasaki, T. Kimura, B. Forghani, and Y. Masuho.** 1991. A human monoclonal antibody against varicella-zoster virus glycoprotein III. *J. Gen. Virol.* **72**:2065–2073.
 48. **Turner, A., B. Bruun, T. Minson, and H. Browne.** 1998. Glycoproteins gB, gD, and gHgL of herpes simplex virus type 1 are necessary and sufficient to mediate membrane fusion in a Cos cell transfection system. *J. Virol.* **72**:873–875.
 49. **Weise, K., H. C. Kaerner, J. Glorioso, and C. H. Schroder.** 1987. Replacement of glycoprotein B gene sequences in herpes simplex virus type 1 strain ANG by corresponding sequences of the strain KOS causes changes of plaque morphology and neuropathogenicity. *J. Gen. Virol.* **68**:1909–1919.
 50. **Weller, T. H.** 1953. Serial propagation in vitro of agents producing inclusion bodies derived from varicella and herpes zoster. *Proc. Soc. Exp. Biol. Med.* **83**:340–346.
 51. **Wilson, D. W., N. Davis-Poynter, and A. C. Minson.** 1994. Mutations in the cytoplasmic tail of herpes simplex virus glycoprotein H suppress cell fusion by a syncytial strain. *J. Virol.* **68**:6985–6993.
 52. **Yao, Z., W. Jackson, B. Forghani, and C. Grose.** 1993. Varicella-zoster virus glycoprotein gpI/gpIV receptor: expression, complex formation, and antigenicity within the vaccinia virus-T7 RNA polymerase transfection system. *J. Virol.* **67**:305–314.
 53. **Yao, Z., W. Jackson, and C. Grose.** 1993. Identification of the phosphorylation sequence in the cytoplasmic tail of the varicella-zoster virus Fc receptor glycoprotein gpI. *J. Virol.* **67**:4464–4473.
 54. **Yokoyama, T., S. Ayabe, H. Miyagi, T. Sugano, A. Otsu, H. Sato, S. Kageyama, T. Fujii, and K. Shiraki.** 2001. Varicella-zoster virus gH:gL contains a structure reactive with the anti-human gamma chain of IgG near the glycosylation site. *J. Gen. Virol.* **82**:331–334.
 55. **Zhu, Z., M. D. Gershon, Y. Hao, R. T. Ambron, C. A. Gabel, and A. A. Gershon.** 1995. Envelopment of varicella-zoster virus: targeting of viral glycoproteins to the *trans*-Golgi network. *J. Virol.* **69**:7951–7959.
 56. **Zhu, Z., Y. Hao, M. D. Gershon, R. T. Ambron, and A. A. Gershon.** 1996. Targeting of glycoprotein I (gE) of varicella-zoster virus to the *trans*-Golgi network by an AYRV sequence and an acidic amino acid-rich patch in the cytosolic domain of the molecule. *J. Virol.* **70**:6563–6575.